A Two-Stage High-Gain Quadratic Boost Converter Using Inverse-Coupled-Inductors for Low Input-Current Ripple

Alwy Muhammad Ravi[1,2*], Herlambang Setiadi[1,2], and Muhammad Zakiyullah Romdlony[1,3]

[1] *Electrical Engineering Study Program, School of Electrical Engineering, Telkom University, Bandung 40257, West Java, Indonesia*

[2] *The University Center of Excellence Sustainable Energy and Climate Change, Telkom University, Bandung 40257, West Java, Indonesia*

[3] *The University Center of Excellence Smart Transportation and Robotics, Telkom University, Bandung 40257, West Java, Indonesia*

[*] *Corresponding author. Email: alwymuhammadravi@telkomuniversity.ac.id*

Abstract— High step-up DC–DC converters are required to interface low-voltage renewable energy sources with higher-voltage dc buses in dc microgrid applications. This paper presents a simulation-based two-stage high-gain DC–DC converter integrating an inverse-coupled-inductor front end with a quadratic boost rear stage. The inverse-coupled front end is employed to reduce source-side input-current ripple and mitigate dc-flux accumulation, thereby lowering the risk of magnetic-core saturation in the front-stage inductors under high-power operation. Compared with uncoupled and direct-coupled configurations, the inverse-coupled arrangement enables ripple-current cancellation between the two input phases, which improves its feasibility for higher-power implementation. The quadratic boost rear stage provides high voltage gain and supports a more stable dc-bus voltage response. Analytical derivations of the operating principle, voltage gain, and input-current ripple ratio are presented, followed by comparative simulation of the three inductor configurations. The results show that the inverse-coupled configuration achieves the lowest average input-current ripple ratio of $6,2089 \times 10^{-4}$, with a minimum value of $2,8042 \times 10^{-6}$ at D_{st1} = 0,5. The converter also produces an output voltage close to 400 V from a 20 V input, corresponding to a voltage gain of approximately 20. These results indicate that the proposed topology offers a promising trade-off between high voltage gain, reduced front-stage magnetic stress, source-side ripple suppression, and output-voltage stability for renewable-energy-fed dc-bus applications.

Keywords— DC–DC Converter; High-Gain Converter; Inverse-Coupled Inductor; Quadratic Boost Converter; Renewable Energy

I. Introduction

Renewable energy sources such as photovoltaic modules, fuel cells, and low voltage battery systems generally provide low dc voltage levels, whereas many practical applications, including dc microgrids and high voltage dc buses, require significantly higher voltage levels. In particular, the effective utilization of power generated by series connected photovoltaic modules typically requires a dc voltage boost in the range of 325 to 400 V for dc bus interfacing [1], [2], [3]. In addition to high voltage gain, converters connected to renewable energy sources are expected to draw a continuous input current with low ripple, since source side current ripple directly affects electromagnetic interference, input filter size, power quality, and the operational lifetime of the source [4], [5], [6]. Therefore, high gain dc to dc converters for renewable energy fed dc buses should not only provide a large voltage conversion ratio but also maintain good input current quality and stable output voltage response.

Conventional boost derived converters usually require operation at an extreme duty ratio to achieve high voltage gain, which increases conduction loss, switching loss, device stress, and reduces practical efficiency [1], [7], [8]. To overcome these limitations, many non-isolated high gain converter topologies have been proposed using coupled inductors, interleaving techniques, voltage multiplier cells, soft switching techniques, and quadratic boost mechanisms [2], [9], [10], [11]. Among these approaches, quadratic boost converters are attractive because they provide a stronger step up characteristic than conventional boost converters while maintaining a relatively compact non isolated structure [7], [9], [10], [12]. Recent quadratic based converters have also incorporated coupled inductors, clamp circuits, and soft switching cells to improve voltage gain, reduce selected device stresses, and enhance power conversion performance [8], [13], [14], [15].

Among non-isolated high gain converter approaches, coupled inductor-based converters require careful classification because magnetic coupling is sometimes associated with galvanic isolation. However, the use of a coupled inductor does not necessarily imply an isolated topology. In non-isolated coupled inductor converters, the magnetic coupling element can be used to improve voltage gain, distribute current, reduce ripple, recycle leakage energy, or improve magnetic utilization, while the input and output sides remain electrically connected [1], [2], [14], [16]. Previous studies have also shown that interleaved and ripple free front-end structures are effective in

Received 24 April 2026, Revised 9 June 2026, Accepted 15 June 2026.

DOI: https://doi.org/10.15294/jte.v18i1.48133

improving source current quality in renewable energy applications [2], [4], [6], [17]. These findings indicate that a front-end structure combining interleaving and magnetic coupling may be useful not only for current sharing and ripple reduction, but also for improving magnetic core utilization in high gain converter applications.

From this perspective, an inverse coupled front end configuration can be considered a feasible approach to reduce source side ripple and magnetic stress in the input stage. In a two-phase structure, the input current is shared between phases, while the ripple current and dc flux components generated by the two windings tend to oppose each other when the inductors are arranged with inverse polarity. Based on this operating principle, the inverse coupled configuration is expected to reduce net input current ripple, mitigate dc flux accumulation, and lower the risk of magnetic core saturation under higher power operation. This characteristic makes the front-end stage more suitable for future high-power implementation, where excessive inductor ripple current and magnetic saturation become critical design constraints. In a two-stage converter, this reduction is also relevant to the intermediate capacitor, which acts as the energy interface between the front-end stage and the rear high gain stage. Since the voltage ripple across the capacitor is related to the integral of the capacitor current ripple, conceptually expressed as $\Delta V_c \approx \frac{1}{C}\int \Delta i_C dt$, reducing front end current ripple is expected to decrease the intermediate capacitor voltage ripple. When the rear stage is implemented using a quadratic boost converter, lower intermediate voltage disturbance can support a more stable output voltage before the converter is connected to the dc bus of a microgrid system.

Based on these research gaps and theoretical considerations, this paper aims to develop a simulation based two stage high gain dc to dc converter using an inverse coupled inductor front end and a quadratic boost rear stage. The inverse coupled inductor front end is intended to suppress source side input current ripple and reduce magnetic stress in the input stage, while the quadratic boost rear stage is used to achieve the required high voltage gain for renewable energy fed dc bus applications. The novelty of this work is not claimed as the invention of the individual subcircuits, since interleaved boost converters, inverse coupled inductors, and quadratic boost converters have been previously reported in the literature [13], [17], [18]. Instead, the main contribution lies in the integration and design-oriented evaluation of these functions in a single non-isolated high gain topology. Specifically, this paper compares uncoupled, direct coupled, and inverse coupled front end inductor configurations under the same high gain operating requirement to evaluate their effects on input current ripple, magnetic behavior, intermediate voltage disturbance, and output voltage stability.

II. Method

A. Operation Principle of The Circuit Topology

The proposed converter is developed as a simulation based two-stage high-gain dc to dc topology consisting of an inverse coupled inductor front-end in Stage 1 and a quadratic boost structure in Stage 2, as shown in Figure 1. The main function of Stage 1 is to improve the source side current quality by reducing the input current ripple and mitigating dc flux accumulation in the front stage magnetic element. Meanwhile, Stage 2 is designed to provide the high voltage gain required for renewable energy fed dc bus applications. By separating the functional roles of the two stages, the proposed converter aims to achieve low source side current ripple and high voltage gain simultaneously [16].

In this topology, the intermediate capacitor C_1 acts as the energy interface between Stage 1 and Stage 2. Therefore, the current and voltage behavior of C_1 is important in determining how disturbances from the front-end stage are transferred to the rear high gain stage. A reduction in the ripple current delivered by Stage 1 is expected to reduce the ripple current imposed on C_1, which can subsequently reduce the intermediate voltage ripple and support a more stable output voltage response. This operating concept is particularly important for dc bus microgrid applications, where output voltage fluctuation may affect dc bus stability.

1) Stage 1: Inverse Coupled Inductir Front-End

Stage 1 can be regarded as a two-phase front-end boost structure in which the input inductors are implemented using an inverse coupled inductor arrangement. This structure is selected because it provides current sharing between two phases and enables ripple current cancellation through magnetic coupling with inverse polarity. In contrast to an isolated converter, the coupled inductor in this stage is not used to provide galvanic isolation. Instead, it is used as a magnetic design element to reduce the net input current ripple and mitigate dc flux accumulation in the front-stage magnetic core.

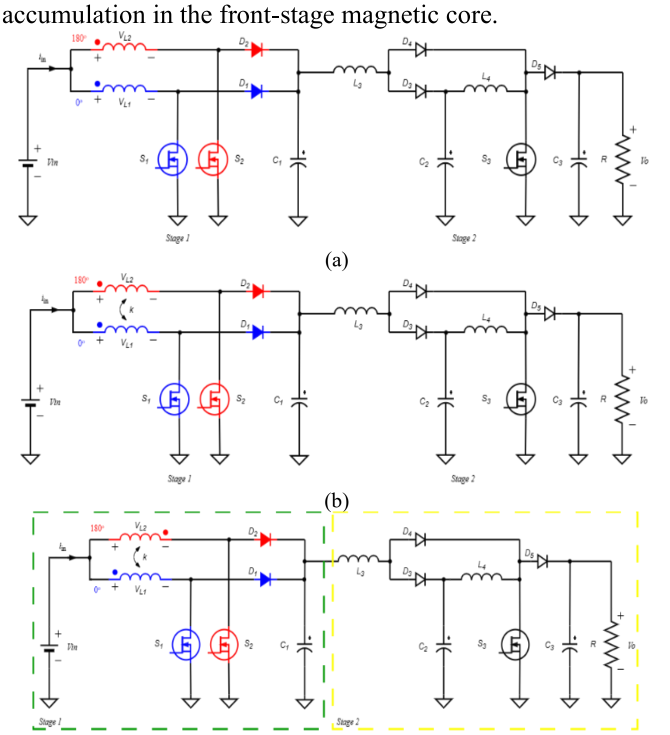

Figure 1. Converter Topology, (a) Uncoupled Inductor, (b) Direct-Coupled Inductor, (c) Proposed Converter Topology – Inverse-Coupled Inductor

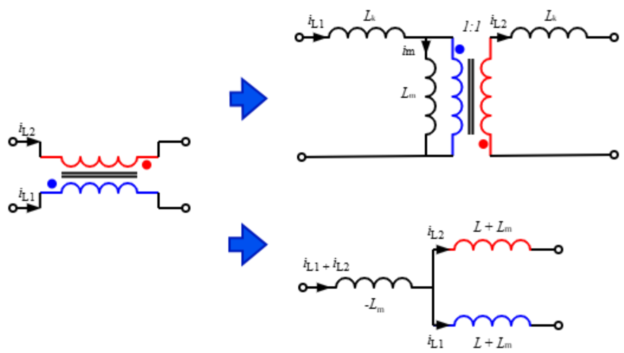

Figure 2. Equivalent Circuit of The Inverse-Coupled Inductor

This stage consists of two inversely coupled inductors L_1 and L_2, power switches S_1 and S_2, diodes D_1 and D_2, and an intermediate capacitor C_1. Under balanced current-sharing conditions, the two windings are assumed to have identical electrical parameters and operate with inverse magnetic polarity. The magnetizing inductance is represented by L_m and an ideal transformer with a 1:1 turn ratio. The leakage inductance and self-inductance of the windings are represented by L_k and L, respectively. The two windings are magnetically coupled with coupling coefficient α and are arranged in an inverse polarity configuration, as illustrated in Figure 2. The equivalent magnetic model of the coupled inductor can be expressed as (1).

$$L = L_k + L_m \tag{1}$$

The coupling relationship is given by (2).

$$\alpha = -\frac{L_m}{L} = -\frac{L_m}{L_k + L_m} \tag{2}$$

By applying Kirchhoff's voltage law to Stage 1 and using (1), the voltage equations of the two windings can be obtained as (3) and (4), respectively.

$$v_{L1} = -L_m\frac{d(i_{L1}+i_{L2})}{dt} + (L+L_m)\frac{di_{L1}}{dt} = L\frac{di_{L1}}{dt} - L_m\frac{di_{L2}}{dt} \tag{3}$$

$$v_{L2} = -L_m\frac{d(i_{L1}+i_{L2})}{dt} + (L+L_m)\frac{di_{L2}}{dt} = -L_m\frac{di_{L1}}{dt} + L\frac{di_{L2}}{dt} \tag{4}$$

where v_{Lj} denotes the windings voltage, with $v_{Lj} = V_{in}$ when S_j is on, and $v_{Lj} = V_{in} - V_{c1}$ when S_j is off $(j = 1,2)$. The inductor currents i_{L1}, i_{L2} can be derived, and the total input current of the coupled-inductor stage is expressed as (5).

$$i_{in} = i_{L1} + i_{L2} \tag{5}$$

The total input current of Stage 1 is obtained from the sum of the two-phase currents based on (5). Since the two windings are arranged with inverse magnetic polarity, the ripple components of i_{L1} and i_{L2} tend to oppose each other. Therefore, the net input current ripple can be significantly reduced when the two-phase currents are balanced. This ripple cancellation mechanism can be expressed as (6).

$$\Delta i_{L1} \approx -\Delta i_{L2} \ thus\ \Delta i_{in} = \Delta i_{L1} + \Delta i_{L2} \approx 0 \tag{6}$$

According to (6), the resulting input current ripple is very small since the currents in Inductors 1 and 2 flow in opposite directions. As a consequence, the magnetic fluxes generated by the two inductors are also opposite, leading to flux cancellation [18]. Figure 3 (a). illustrates the current waveform of Stage 1 and shows the ripple cancellation mechanism produced by the inverse-coupled inductor arrangement. This behavior is beneficial for high power operation because the reduction of dc flux accumulation can lower magnetic stress and decrease the possibility of core saturation in the front-stage inductor. The ripple current ratio is determined from the current variation during the on-state interval. During the on state of switches S_1 and S_2, the slope of the input current is given by (7).

$$\frac{di_{in}}{dt\_on} = \frac{2V_{in}}{L(1-\alpha)} \tag{7}$$

and the corresponding input current ripple during the on-state interval is given by (8).

$$\Delta i_{in} = \frac{2V_{in}}{L(1-\alpha)}D_{st1}T_1 \tag{8}$$

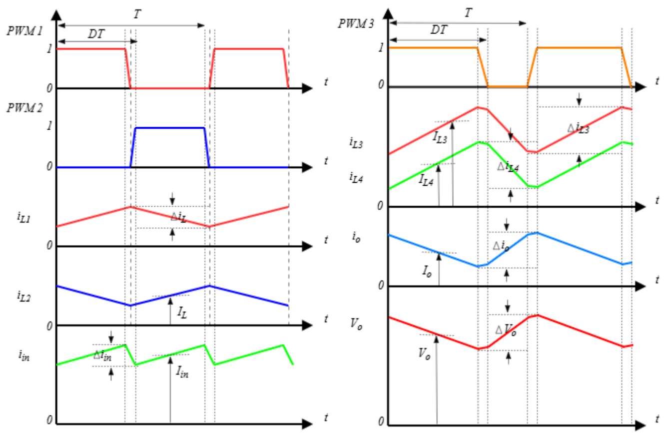

(a) (b)

Figure 3. CCM Mode Current Waveform and Switching Pattern of (a) Stage 1, (b) Stage 2

The output voltage of Stage 1 follows the same voltage conversion principle as a conventional boost converter and can be written as (9).

$$V_{c1} = \frac{V_{in}}{1 - D_{st1}} \tag{9}$$

Equation (9) defines the intermediate capacitor voltage, which also serves as the input voltage of Stage 2. Since the C_1 serves as the energy interface between the inverse coupled inductor front end and the quadratic boost rear stage, the ripple current imposed on C_1 affects the intermediate voltage V_{c1} and can influence the output voltage response of the converter. The capacitor current can be conceptually expressed as the difference between the current delivered by Stage 1 and the current demanded by Stage 2 based on (10).

$$i_{C1} = i_{stage1} - i_{stage2} \tag{10}$$

where i_{stage1} represents the current supplied by the front-end stage to the intermediate capacitor, and i_{stage2} represents the current drawn by the quadratic boost rear stage. The ripple component of the capacitor current can therefore be expressed as (11).

$$\Delta i_{C1} = \Delta i_{stage1} - \Delta i_{stage2} \tag{11}$$

The voltage ripple across C_1 is related to the integral of the capacitor current ripple. Hence, the intermediate capacitor voltage ripple can be approximated as (12).

$$\Delta V_{c1} \approx \frac{1}{C_1}\int \Delta i_{C1}dt \tag{12}$$

Equation (12) shows that reducing the ripple current imposed on C_1 can reduce the intermediate voltage ripple. Since the inverse coupled inductor front end is designed to suppress Δi_{stage1} through ripple current cancellation, the resulting Δi_{C1} and ΔV_{c1} are expected to decrease. This provides a theoretical explanation of why the proposed front-end structure can support a more stable intermediate voltage. The output voltage of the quadratic boost rear stage can be expressed as (13).

$$V_o = G_2 V_{c1} \tag{13}$$

$$\Delta V_o = G_2 \Delta V_{c1} \tag{14}$$

where G_2 is the gain of stage 2. For small signal ripple propagation, the output voltage ripple caused by the intermediate voltage ripple and can be approximated in (14). Substituting (12) into (14), the relationship between capacitor current ripple and output voltage ripple can be conceptually written as (15).

$$\Delta V_o = G_2\frac{1}{C_1}\int \Delta i_{C1}dt \tag{15}$$

TABLE I. CONVERTER SPECIFICATIONS

Parameter	Value
Input Voltage V_{in}	20 V
Output Voltage V_{out}	400 V
Rated Power P	160 W
Coupling Coefficient α	0,85
Switching Frequency Stage 1 f_{s1}	50 kHz
Switching Frequency Stage 2 f_{s2}	100 kHz
Current Ripple ΔI	10 %
Voltage Ripple ΔV	10 %

This relationship indicates that any ripple appearing at the intermediate capacitor can be transferred and scaled by the quadratic boost stage. Therefore, reducing the front-end current ripple is important not only for source current quality, but also for reducing the disturbance to the output voltage. This supports the use of the inverse coupled inductor front end before the quadratic boost rear stage, especially for dc bus microgrid applications that require stable output voltage.

2) Stage 2: Quadratic Boost Rear Stage

Stage 2 is implemented as a quadratic boost rear stage to provide the required high voltage gain. The input of this stage is supplied by the intermediate capacitor C_1, whose voltage is denoted as V_{c1}. The rear stage consists of inductors L_3 and L_4, capacitors C_2 and C_3, diodes D_3, D_4 and D_5, and switch S_3. Its main function is to step up the intermediate voltage to the required dc bus voltage level.

When switch S_3 is turned on, energy is stored in the inductors of the quadratic boost stage. When S_3 is turned off, the stored energy is transferred through the diode capacitor network to the output capacitor and load. By applying the volt-second balance principle to L_3 and L_4, the voltage conversion relation of Stage 2 can be derived. Since Stage 2 has a quadratic voltage gain characteristic, a high output voltage can be obtained without relying solely on an extreme duty ratio in Stage 1 based on (16) and (17).

$$V_{L3(on)} = V_{c1}, V_{L3(off)} = V_{c1} - V_{c2} \tag{16}$$

Thus:

$$V_{c2} = \frac{V_{c1}}{1 - D_{st2}} \tag{17}$$

Similarly, by applying the volt-second balance principle to L_4, the output voltage relation can be obtained as (18) and (19).

$$V_{L4(on)} = V_{c2}, V_{L4(off)} = V_{c2} - V_o \tag{18}$$

Thus:

$$V_o = \frac{V_{c2}}{1 - D_{st2}} \tag{19}$$

Substituting (17) to (19), the output voltage of Stage 2 is given by (20).

$$V_o = \frac{V_{c1}}{(1 - D_{st2})^2} \tag{20}$$

Since the output voltage of Stage 1 is defined by (9), the overall voltage gain of the proposed converter becomes (21).

$$\frac{V_o}{V_{in}} = \frac{1}{(1 - D_{st1})(1 - D_{st2})^2} \tag{21}$$

The overall gain based on (21) expression shows that the proposed converter combines the boost characteristic of Stage 1 and the quadratic characteristic of Stage 2. The front-end inductor configuration mainly affects the source side input current ripple, dc flux behavior, and intermediate voltage disturbance, whereas the steady state voltage gain is primarily determined by the cascaded boost quadratic boost conversion mechanism. Therefore, the inverse coupled inductor front end is not intended to increase the voltage gain directly, but to improve the input-current quality and reduce disturbance before the energy is processed by the high gain rear stage. This high step-up behavior is consistent with recent coupled inductor and voltage multiplier based high gain converter developments [19].

3) Ripple Current Ration

This high voltage gain achieved by the proposed converter also influences the final input ripple ratio, since the average input current is determined by the output power demand [20]. Under ideal conditions, the input and output power are equal, and the average input current can be obtained from (22).

$$P_{in} = P_{out} \leftrightarrow I_{in} = \frac{V_o^2}{V_{in}R_{out}} \tag{22}$$

By substituting (21) into (22), the average input current is expressed in (23).

$$I_{in} = \frac{V_{in}}{R_{out}(1 - D_{st1})^2(1 - D_{st2})^4} \tag{23}$$

After obtaining the average input current, the ripple ratio r_{in} can be calculated using (24) and (25). A lower value of r_{in} indicates a lower ripple component relative to the average input current. In the proposed converter, the inverse coupled inductor configuration is expected to produce the smallest r_{in} because the ripple components of the two input phases tend to cancel each other. This reduced input current ripple can also decrease the ripple current imposed on C_1 as described in the intermediate capacitor ripple analysis.

$$r_{in} = \frac{\Delta i_{in}}{I_{in}} \tag{24}$$

$$r_{in} = \frac{2T_{st1}D_{st1}R_{out}(1 - D_{st1})^2(1 - D_{st2})^4}{L(1 - \alpha)} \tag{25}$$

B. Design Details

The design procedure is carried out based on the specified simulation operating conditions, which are summarized in Table I. The component values are calculated using the analytical equations derived in the previous subsections. These calculated values are used for comparative simulation among the uncoupled, direct coupled, and inverse coupled front-end configurations. The same design basis will also be used for the future hardware prototype, particularly for the fabrication of the coupled inductor according to the theoretical inductance and coupling requirements [21]. For stage-1, the inductances L_1 and L_2 are designed form the input current ripple during the on-state interval as based on (26).

$$L = \frac{2V_{in}}{\Delta i_{in}(1 - \alpha)} D_{st1}T_1 \tag{26}$$

Unlike uncoupled inductors, coupled inductors also require the calculation of mutual inductance based on (2). The mutual inductance is determined from the coupling coefficient α related to the coupling relationship. To compare the performance of the inverse coupled inductor configuration, two additional cases are considered, namely uncoupled inductors and direct coupled inductors. These two configurations are used as references to validate the influence of magnetic coupling on input current ripple and overshoot behavior. For the uncoupled inductors case, no mutual inductance exists, and the inductor value is determined by equation (27).

$$L = \frac{2V_{in}}{\Delta i_{in}} D_{st1}T_1 \tag{27}$$

For direct coupled inductor case, the coupling coefficient appears with a positive sign. In contrast, the negative sign in the inverse coupled configuration reflects the opposite magnetic polarity between the two windings on (28).

$$L = \frac{2V_{in}}{\Delta i_{in}(1+\alpha)} D_{st1} T_1 \quad (28)$$

The capacitor (C_1) in Stage 1 is calculated using the conventional boost-capacitor relation on (29).

$$C_1 = \frac{I_{C_1} D_{st1}}{f_{s1} \Delta V_{C_1}} \quad (29)$$

For Stage 2, the values of inductors L_3 and L_4 are obtained from the on-state voltage relations in (16) and (18), respectively, as (30) and (31).

$$L_3 = \frac{V_{C_1} D_{st2}}{\Delta i_{L3} f_{s2}} \quad (30)$$

$$L_4 = \frac{V_{C_2} Dst_2}{\Delta i_{L4} f_{s2}} \quad (31)$$

In contrast to the inductance design, the capacitor values are determined from the electric-charge relationship $Q = C \times \Delta V$, which gives on (32) and (33).

$$C_2 = \frac{I_{C_2} D_{st2}}{f_{s2} \Delta V_{C_2}} \quad (32)$$

$$C_3 = \frac{I_{C_3} D_{st2}}{f_{s2} \Delta V_{C_3}} \quad (33)$$

Finally, the load resistance is calculated from the output power relation as (34).

$$R_{out} = \frac{V_o^2}{P_{out}} \quad (34)$$

III. RESULTS AND DISCUSSION

This section presents the analytical and simulation-based evaluation of the proposed two stage high gain dc to dc converter. The discussion focuses on the calculated component values, the comparison of uncoupled, direct coupled, and inverse coupled front end inductor configurations, input current ripple reduction, dc flux cancellation behavior, intermediate capacitor voltage disturbance, efficiency tendency, and output voltage stability. Since the present work is based on analytical derivation and simulation verification, the results are intended to evaluate the operating concept and comparative performance of the proposed topology. Experimental validation is not included in this manuscript because the hardware prototype is still under development, including troubleshooting and fabrication of the coupled inductor according to the theoretical design. Through these evaluations, the proposed topology is assessed to verify the hypothesis that the inverse coupled inductor front end can suppress source side input current ripple while preserving high voltage gain [22].

A. Component Design and Simulation Conditions

The component values used in the simulation are obtained from the analytical design equations described in the previous section. The converter is designed to step up a 20 V input voltage to an output voltage close to 400 V under the specified operating condition. To ensure a fair comparison, the uncoupled, direct coupled, and inverse coupled front end configurations are evaluated using the same input voltage, output voltage target, rated power, switching frequencies, and duty cycle range in accordance with Table I.

The main difference among the three cases lies in the magnetic arrangement of the Stage 1 inductors. In the uncoupled case, no mutual inductance exists between the two input inductors. In the direct coupled case, the magnetic flux components tend to reinforce each other. In contrast, the inverse coupled configuration uses opposite magnetic polarity, allowing the ripple current and dc flux components to partially cancel each other under balanced current sharing conditions. These differences provide the basis for evaluating the influence of magnetic coupling on the ripple-reduction capability of the converter and will later be used for comparison in the prototype implementation.

B. Input Current Ripple Ratio Comparison

The performance of the three Stage 1 inductor configurations is evaluated based on the input current ripple ratio. Since the rear quadratic boost stage is kept identical for all cases, the difference in r_{in} mainly reflects the influence of the front-end magnetic configuration. As summarized in Table III and illustrated in Figure 4, the Stage 1 duty cycle is varied within the investigated range $0{,}41 \leq D_{st1} \leq 0{,}59$ while the Stage 2 duty cycle is adjusted to maintain the required voltage gain from (21). The inverse coupled configuration produces the lowest average input current ripple ratio among the investigated cases. This result indicates that arranging the two input inductors with inverse magnetic polarity effectively reduces the net ripple of the input current. The lower ripple ratio is obtained because the ripple current generated by the two front-end phases tend to cancel each other under balanced current sharing conditions. This result supports the role of Stage 1 as a source current conditioning stage. Therefore, the advantage of the inverse coupled front-end is not only related to the numerical reduction of r_{in}, but also to the improvement of source current quality before the energy is processed by the quadratic boost rear stage. The average rin of the inverse coupled case is $6{,}2089 \times 10^{-4}$, while the uncoupled and direct coupled cases produce $76{,}4741 \times 10^{-4}$ and $75{,}2196 \times 10^{-4}$, respectively. At D_{st1}= 0,5, the inverse coupled configuration reaches the minimum ripple ratio of $2{,}8042 \times 10^{-6}$.

As shown in Figure 5, the inverse coupled inductor configuration produces the most stable input current response and the smallest ripple among the three investigated cases. In general, both direct-coupled and inverse-coupled inductors can reduce the input current ripple more effectively than uncoupled inductors because magnetic coupling allows interaction between the two windings, which is absent in the uncoupled case. According to (6), the input current ripple is determined by the sum of the ripple components in the two inductors. In the inverse-coupled configuration, these ripple components tend to cancel each other, resulting in a substantially lower net ripple. This behavior directly supports the main objective of Stage 1 and validates the use of inverse magnetic coupling as a source-current ripple suppression mechanism. The DC flux cancellation effect is clearly evident in the inductor current simulation results for all three types of inductors in the following subsection.

TABLE II. COMPARISON OF COMPONENT DESIGN

Parameter	Uncouple Inductor	Direct Couple Inductor	Inverse Couple Inductor
Inductor Stage 1	L_1 & L_2= 500 μH	L_1 & L_2= 270 μH	L_1 & L_2= 3.33 mH
Mutual Inductance	-	230 μH	-2.83 mH
Capacitor 1 Stage 1		10 μF	
Inductor 3 Stage 2		684 μH	
Capacitor 2 Stage 2		1 μF	
Inductor 4 Stage 2		6.85 mH	
Capacitor 3 Output		1 μF	
Resistance Output		1000 Ω	

TABLE III. INPUT CURRENT RIPPLE RATIO

Duty Cycle Stage 1 (D_{st1})	Duty Cycle Stage 2 (D_{st2})	Input Current Ripple Ratio (r_{in})		
		Uncoupled Inductor	Direct-Coupled Inductor	Inverse-Coupled Inductor
0.41	0.709	0.01214605	0.01190095	0.00098646
0.42	0.706	0.01105145	0.01078541	0.00089694
0.43	0.704	0.00975489	0.00948592	0.00079143
0.44	0.701	0.00853840	0.00828010	0.00069377
0.45	0.698	0.00726933	0.00701107	0.00059000
0.46	0.696	0.00585318	0.00560827	0.00047519
0.47	0.693	0.00447150	0.00425091	0.00036350
0.48	0.690	0.00301980	0.00282582	0.00024508
0.49	0.687	0.00151084	0.00134146	0.00012269
0.50	0.684	0.00003447	0.00021046	0.00000280
0.51	0.681	0.00162682	0.00172121	0.00013243
0.52	0.677	0.00332630	0.00338217	0.00026995
0.53	0.674	0.00505119	0.00507282	0.00041002
0.54	0.670	0.00690467	0.00689024	0.00056031
0.55	0.667	0.00874539	0.00869249	0.00070972
0.56	0.663	0.01076449	0.01053528	0.00087300
0.57	0.659	0.01286896	0.01278928	0.00104373
0.58	0.655	0.01507476	0.01489621	0.00122219
0.59	0.651	0.01728822	0.01723716	0.00140776

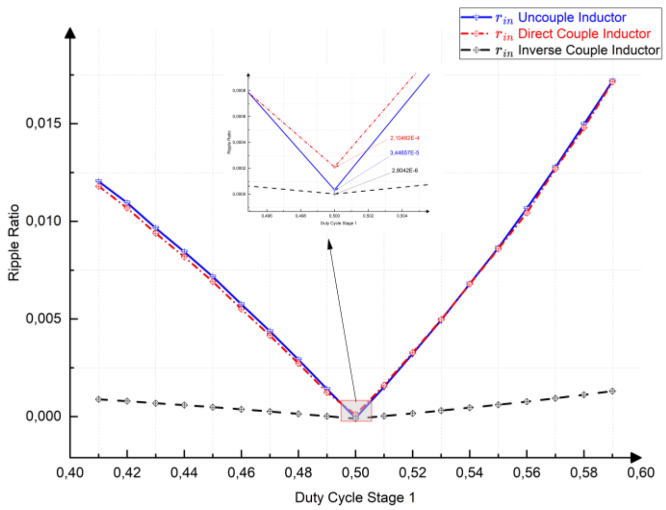

Figure 4. Ripple Input Current Ratio on Stage 1

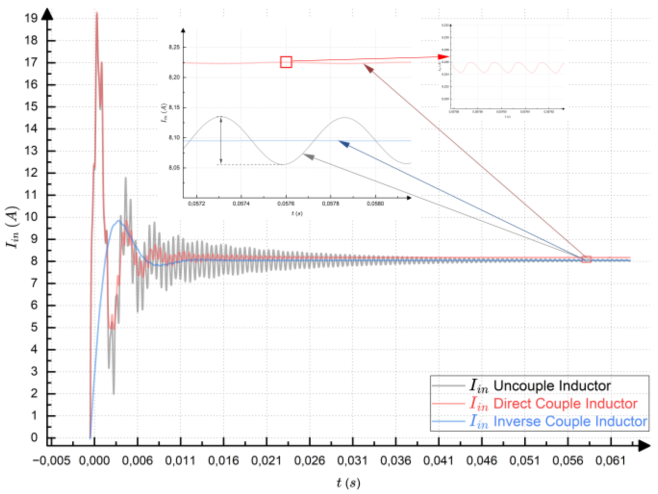

Figure 5. Input Current Response

C. Comparison of DC Flux Cancellation

The dc flux cancellation effect is examined to evaluate how the coupled-inductor configuration affects current stress in the magnetic core when higher power is applied. Figure 6 presents the simulated inductor current waveforms for the three investigated configurations under an output power of 160 W.

Figure 6(a) shows the uncoupled inductor case, where no dc flux cancellation occurs because no magnetic coupling exists between the two inductors. Consequently, the current ripple remains relatively large. In the direct coupled inductor case shown in Figure 6(b), the magnetic fluxes accumulate instead of cancelling each other, which increases the risk of core saturation and results in a larger inductor current ripple. In contrast, the inverse coupled inductor configuration in Figure 6(c) provides the most favourable condition for high-power operation. In this case, the dc fluxes generated in the two windings oppose each other and tend to cancel, resulting in a smaller inductor current ripple and lower magnetic stress. This dc flux cancellation behavior is an important advantage of the proposed converter, since it not only improves input-current quality but also enhances the suitability of the converter for higher-power applications.

D. Efficiency Tendency and Switching Loss Consideration

The use of a two-phase front-end introduces two active switches in Stage 1. Compared with a single switch boost front end, this configuration may increase the number of switching devices and can potentially add switching loss components. However, the objective of Stage 1 in this work is not to minimize the switching device count, but to improve source current quality by reducing input current ripple and mitigating dc flux accumulation in the front stage magnetic core. In a single switch boost front-end, the entire input current is processed by one switch and one inductor, which may increase the current burden and input current ripple under higher power operation. In contrast, the two-phase inverse coupled front-end allows current sharing between phases, while the inverse magnetic coupling enables ripple current cancellation and dc flux cancellation. Therefore, the proposed front-end should be understood as a design trade-off between switching device count, source current quality, and magnetic core utilization. This consideration is consistent with previous studies reporting that interleaved and coupled inductor-based converters can reduce input current ripple and improve current sharing in renewable energy applications [2], [6], while inverse coupled inductors can reduce dc flux accumulation and magnetic saturation tendency in interleaved boost converters [18]. The influence of the inverse coupled inductor configuration on input current ripple and efficiency tendency is shown in Figure 7. Compared with the direct coupled inductor configuration, the inverse coupled case shows a better efficiency tendency in the investigated power range.

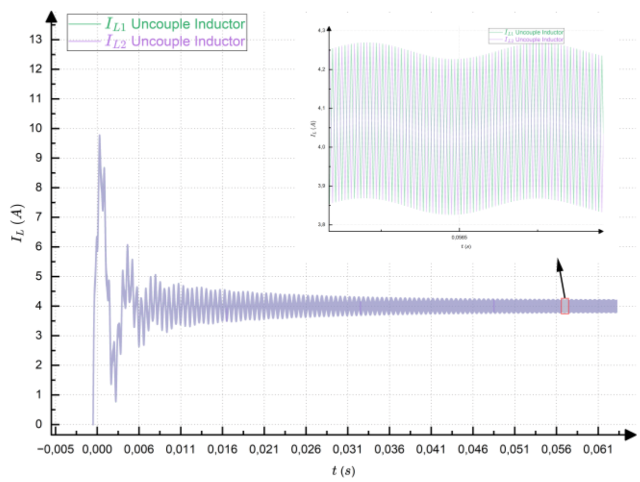

(a)

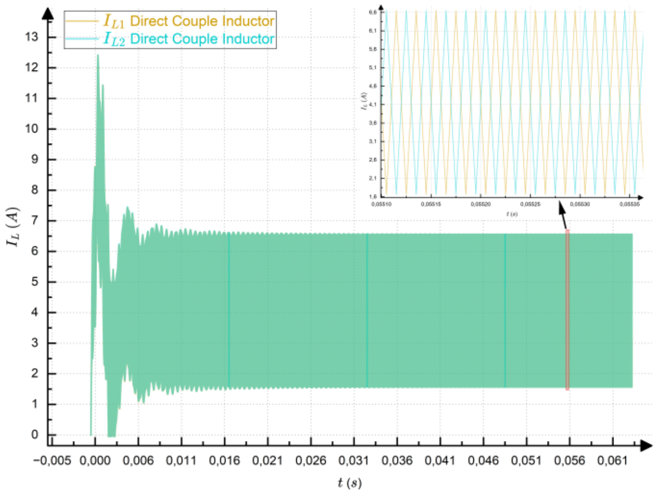

(b)

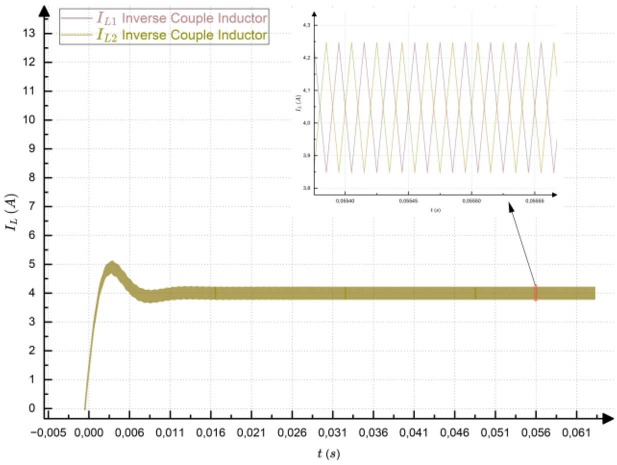

(c)

Figure 6. Ripple Current of Inductor, (a) Uncoupled Inductor, (b) Direct-Coupled Inductor, (c) Inverse-Coupled Inductor

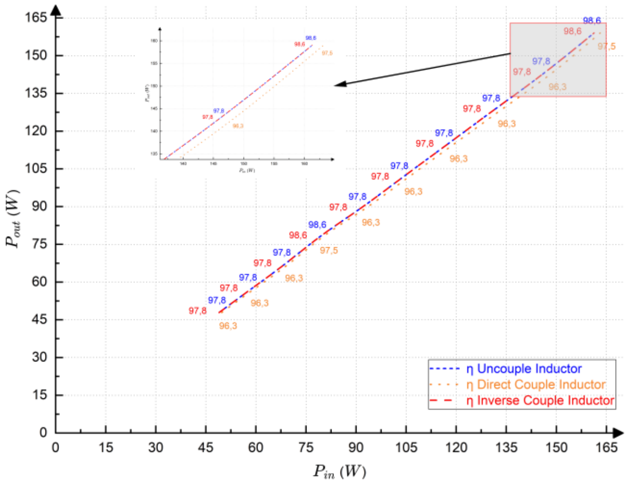

Figure 7. Efficiency of Converter

The efficiency of the inverse coupled configuration is also close to that of the uncoupled case. However, although the uncoupled configuration can provide comparable efficiency at lower power levels, its input current ripple becomes considerably larger as the converted power increases. As a result, the inverse coupled inductor configuration offers a better overall compromise between efficiency and ripple suppression, making it more suitable for practical renewable energy fed applications [23].

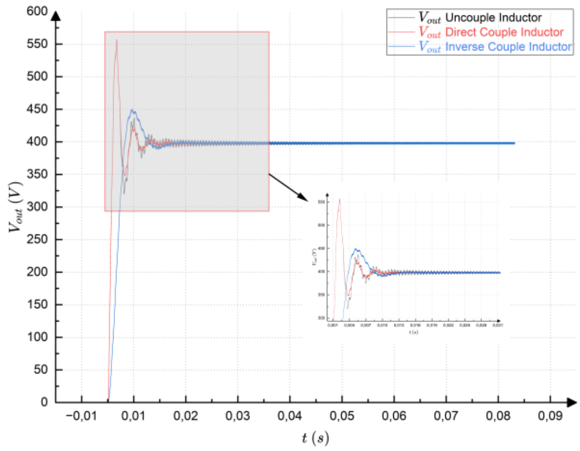

Figure 8. Output Voltage Stability

E. Voltage Gain Profile and Comparison with Related High Gain Converter Topologies

To further clarify the high gain characteristic, the proposed converter is compared with related high gain converter topologies using their voltage gain expressions or reported gain characteristics. The comparison focuses on how each topology achieves voltage amplification. In coupled inductor-based converters, the voltage gain is generally extended by the winding turns ratio and duty cycle. In quadratic boost-based converters, the voltage gain is mainly increased by the squared denominator term. In contrast, the proposed converter separates the function of the two stages. The inverse coupled front end contributes the boost gain while mainly improving input current ripple and magnetic behavior, whereas the quadratic boost rear stage provides the dominant high voltage conversion.

The voltage gain characteristic of the proposed converter is evaluated using the overall gain expression in (21). This expression shows that the proposed converter obtains its high gain from the multiplication of the Stage 1 boost gain and the Stage 2 quadratic boost gain. The gain profile is evaluated under different duty cycle combinations. Although D_{st1} is varied, D_{st2} is adjusted to maintain the required high voltage gain. As shown in Table IV, the related converters achieve high voltage gain using different mechanisms. Coupled inductor-based converters increase gain through winding turns ratio and magnetic coupling, while quadratic boost-based converters increase gain through the squared denominator term. Some ripple free or low ripple converters mainly focus on improving the input current characteristic, but their gain expressions usually depend on additional cells, coupled inductors, or multiplier circuits.

Compared with those topologies, the proposed converter uses a simpler two stage gain structure. The Stage 1 boost relation contributes the term $\frac{1}{1-D_{st1}}$ while the Stage 2 quadratic boost relation contributes the term $\frac{1}{(1-D_{st2})^2}$. Therefore, the proposed converter separates the source current conditioning function and the voltage boosting function.

F. Output Voltage Stability and Suitability for DC Bus Microgrid

The output voltage response is evaluated to observe the influence of the front-end configuration on the dc bus voltage behavior. The inverse coupled configuration provides the most stable output voltage response among the investigated configurations and does not produce significant overshoot. This behavior is consistent with the intermediate capacitor analysis, where the voltage ripple across C_1 is related to the integral of the capacitor current ripple. A lower input current ripple reduces the disturbance imposed on C_1. Since the quadratic boost rear stage processes the intermediate voltage to generate the final output voltage, reducing the intermediate voltage disturbance helps suppress the fluctuation propagated to the output side. This characteristic is desirable before the converter is connected to the dc bus of a microgrid system, because excessive output voltage fluctuation may affect dc bus voltage regulation and system stability.

TABLE IV. VOLTAGE GAIN PROFILE PROPOSED CONVERTER

Ref.	Converter Type	Voltage Gain Characteristic	Gain Extension Mechanism
[1]	Coupled inductor high step-up converter	$\frac{2(N+1)}{1-D}$ under ideal condition	Gain is increased by duty cycle D and coupled inductor turns ratio N
[2]	Interleaved three winding coupled inductor converter	$\frac{\begin{pmatrix}5+5N)+\\N(N-2D\end{pmatrix}}{1-D}$	Gain is extended using interleaving, three winding coupled inductors, and voltage multiplier cells
[5]	Quadratic boost converter with less input ripple	Quadratic voltage gain characteristic, generally related to $\frac{1}{(1-D)^2}$	Gain is obtained from quadratic boost operation
[6]	Ripple free high gain converter	$\frac{2+N+2nk}{1-D}$	Gain is extended by voltage lift capacitor, diode capacitor multiplier cells, coupled inductors, and turns ratio
[10]	Improved non isolated QBC	$\frac{(1+n)(2-D)}{(1-D)^2}$ for the simplified equal winding case	Gain is improved by integrating a triple winding coupled inductor into a QBC network
[13]	Quadratic extended duty ratio boost converter	Reported conversion ratio around 30 at duty ratio close to 0,64 in interleaved configuration	Gain is extended by combining extended duty ratio boost and quadratic boost operation
[14]	Coupled inductor based quadratic step-up converter	$\frac{[2+(n+m)k]+(n-mk)D}{(1-D)^2}$	Gain is extended by coupled inductor parameters, duty cycle, and quadratic conversion
[17]	Ripple free input current step-up converter	Reported as a single switch high voltage gain converter with ripple free input current	Gain is extended using coupled inductor, voltage multiplier circuit, auxiliary circuit, and regenerative clamp
Proposed	Two stage inverse coupled inductor and QBC	$\frac{1}{[(1-D_{st1})(1-D_{st2})^2]}$	Stage 1 provides boost gain and ripple cancellation; Stage 2 provides quadratic voltage gain

TABLE V. OUTPUT VOLTAGE CONVERTER

Input Voltage V_i (V)	Output Voltage V_o (V)					
	Uncoupled Inductor		Direct-Coupled Inductor		Inverse-Coupled Inductor	
	$V_o(V)$	$Gain$	$V_o(V)$	$Gain$	$V_o(V)$	$Gain$
11	218,865	19,897	218,861	19,896	218,865	19,897
12	238,758	19,897	238,754	19,896	238,758	19,897
13	258,658	19,897	258,654	19,896	258,658	19,897
14	279,150	19,939	279,146	19,939	279,150	19,939
15	298,439	19,896	298,434	19,896	298,439	19,896
16	318,308	19,894	318,303	19,894	318,308	19,894
17	338,238	19,896	338,233	19,896	338,238	19,896
18	358,153	19,897	358,147	19,897	358,153	19,897
19	378,036	19,897	378,029	19,896	378,036	19,897
20	398,763	19,938	398,758	19,938	398,763	19,938

As listed in Table V, the converter maintains a voltage gain of approximately 20 for all three Stage 1 inductor configurations, regardless of whether uncoupled, direct-coupled, or inverse-coupled inductors are employed. The ability to produce an output voltage close to 400 V from a 20 V input confirms that the proposed converter is capable of meeting the voltage requirement of a dc bus in a microgrid system [24], [25]. Therefore, the converter not only achieves low input-current ripple but also preserves the high voltage gain needed for renewable energy fed dc bus interfacing.

Figure 8 shows the output voltage stability of the converter for the three investigated Stage 1 inductor configurations. It can be seen that the inverse coupled inductor configuration provides the most stable output voltage response and does not produce significant overshoot. This behavior is highly desirable for dc bus applications, since large transient overshoots may disturb the stability of the microgrid when the converter is directly connected to the dc bus. The use of an inverse coupled inductor therefore improves the converter performance in two important aspects. First, it reduces input current ripple and improves the magnetic behavior of the front stage. Second, it contributes to a more stable output voltage response, which enhances the converter's suitability for practical dc microgrid applications.

IV. CONCLUSION

This paper presented a simulation based two stage high gain dc to dc converter integrating an inverse coupled inductor front end with a quadratic boost rear stage. The front-end stage was designed to suppress source side input current ripple and mitigate dc flux accumulation, while the quadratic boost rear stage was used to provide the required high voltage gain for renewable energy fed dc bus applications. The simulation results showed that the inverse coupled configuration achieved the lowest input current ripple ratio among the investigated configurations. The average input current ripple ratio was $6{,}2089 \times 10^{-4}$, with a minimum value of $2{,}8042 \times 10^{-6}$ at $D_{st1} = 0{,}5$. The converter also maintained a voltage gain of approximately 20 and produced an output voltage close to 400 V from a 20 V input. These results indicate that the proposed topology provides a favorable trade off among high voltage gain, input current ripple suppression, improved front stage magnetic behavior, and output voltage stability. The present work is limited to analytical derivation and simulation-based verification. Experimental validation, detailed semiconductor voltage and current stress analysis, and quantitative switching loss evaluation will be carried out in future work together with the hardware prototype implementation.

ACKNOWLEDGEMENT

The authors would like to express their sincere gratitude to Telkom University for supporting this work through internal research funding. The authors also gratefully acknowledge the Electrical Engineering Study Program, the Control, Electronics and Intelligent Systems Research Group, and the Center of Excellence Sustainable Energy and Climate Change, Telkom University, for providing the academic environment, research facilities, and opportunities that made the development of this work possible.

REFERENCES

[1] Ghaffarpour Sadighi, H., Afjei, S.E. and Salemnia, A. (2020), High step-up DC–DC converter based on coupled-inductor for renewable energy systems. IET Power Electronics, 13: 4315-4324. https://doi.org/10.1049/iet-pel.2020.0310

[2] Hashemzadeh, S.M., Al-Hitmi, M.A., Aghaei, H., Marzang, V., Iqbal, A., Babaei, E., Hosseini, S.H., Islam, S.: An ultra-high voltage gain interleaved converter based on three-winding coupled inductor with reduced input current ripple for renewable energy applications. IET Renew. Power Gener.18, 141–151 (2024). https://doi.org/10.1049/rpg2.12906

[3] Hosseini, S.JA., Hasanpour, S., Shahgholian, G. et al. A new ultra-high voltage gain DC/DC converter based on coupled-inductor. Sci Rep 15, 5330 (2025). https://doi.org/10.1038/s41598-025-90093-1

[4] Mansour, A.S., Amer, AH.H., El-Kholy, E.E. et al. High gain DC/DC converter with continuous input current for renewable energy applications. Sci Rep 12, 12138 (2022). https://doi.org/10.1038/s41598-022-16246-8

[5] M. Ashok Bhupathi Kumar and V. Krishnasamy, "Quadratic Boost Converter With Less Input Current Ripple and Rear-End Capacitor Voltage Stress for Renewable Energy Applications," in IEEE Journal of Emerging and Selected Topics in Power Electronics, vol. 10, no. 2, pp. 2265-2275, April 2022, doi: 10.1109/JESTPE.2021.3122354

[6] Valarmathy, A.S., Prabhakar, M. Non-isolated high gain DC–DC converter with ripple-free source current. Sci Rep 14, 973 (2024). https://doi.org/10.1038/s41598-024-51584-9

[7] S. V. K. Naresh, S. Peddapati and M. L. Alghaythi, "Non-Isolated High Gain Quadratic Boost Converter Based on Inductor's Asymmetric Input Voltage," in IEEE Access, vol. 9, pp. 162108-162121, 2021, doi: 10.1109/ACCESS.2021.3133581

[8] Elghabsi, F., Sahid, M.R., Ayop, R. et al. High gain and high efficiency soft switching quadratic boost converter for renewable energy applications. Sci Rep 15, 36238 (2025). https://doi.org/10.1038/s41598-025-20207-2

[9] Hasanpour, S.: A novel soft-switching quadratic high voltage gain trans-inverse DC/DC converter. IET Power Electron.17, 2714–2729 (2024). https://doi.org/10.1049/pel2.12716

[10] Izadi, M., Mosallanejad, A., Eshkevari, A.L.: A non-isolated quadratic boost converter with improved gain, high efficiency, and continuous input current. IET Power Electron.16, 193–208 (2023). https://doi.org/10.1049/pel2.12376

[11] S. Hasanpour and S. S. Lee, "A New Quadratic DC/DC Converter With Ultrahigh Voltage Gain," in IEEE Transactions on Power Electronics, vol. 39, no. 7, pp. 8800-8812, July 2024, doi: 10.1109/TPEL.2024.3385411.

[12] H. -D. Liu, A. S. Jana and C. -H. Lin, "An Improved High Gain Continuous Input Current Quadratic Boost Converter for Next–Generation Sustainable Energy Application," in IEEE Transactions on Circuits and Systems II: Express Briefs, vol. 71, no. 5, pp. 2839-2843, May 2024, doi: 10.1109/TCSII.2022.3233555.

[13] A. Gupta, N. Korada and R. Ayyanar, "Quadratic-Extended-Duty-Ratio Boost Converters for Ultra High Gain Application With Low Input Current Ripple and Low Device Stress," in IEEE Transactions on Industry Applications, vol. 59, no. 1, pp. 938-948, Jan.-Feb. 2023, doi: 10.1109/TIA.2022.3207132.

[14] Izadi, M., Mosallanejad, A., Eshkevari, A.L.: An improved coupled inductor-based quadratic step-up DC–DC converter with a high step-up factor and reduced voltage overshoot on the power switch. IET Power Electron.17, 986–1004 (2024). https://doi.org/10.1049/pel2.12567

[15] Hasanpour, S., Nouri, T. A new quadratic step-up DC-DC converter with low voltage and current stresses. Sci Rep 15, 38712 (2025). https://doi.org/10.1038/s41598-025-23433-w

[16] Aghakhanlou, P., Falahi, F., Nadermohammadi, A. et al. New structure of step-up DC-DC converter based on three winding coupled inductor with high gain capability featuring integrated renewable energy applications. Sci Rep 14, 31959 (2024). https://doi.org/10.1038/s41598-024-83502-4

[17] S. Hasanpour and S. S. Lee, "New Step-Up DC/DC Converter With Ripple-Free Input Current," in IEEE Transactions on Power Electronics, vol. 39, no. 2, pp. 2811-2821, Feb. 2024, doi: 10.1109/TPEL.2023.3336005.

[18] Z. Wang, C. Li, Z. Zheng, H. Jiang and Z. Huang, "A DC Flux Cancellation Design Method for Inverse-Coupled Inductors Used in Interleaved Boost Converters," in IEEE Transactions on Transportation Electrification, vol. 10, no. 2, pp. 2956-2964, June 2024, doi: 10.1109/TTE.2023.3302803.

[19] He, Y., Sun, X., Liu, S., Wang, N.: High step-up DC–DC converter using coupled inductor voltage multiplier cell and differential connection method. IET Power Electron.16, 542–557 (2023). https://doi.org/10.1049/pel2.12406

[20] Mansour, A.S., Zaky, M.S. A new extended single-switch high gain DC–DC boost converter for renewable energy applications. Sci Rep 13, 264 (2023). https://doi.org/10.1038/s41598-022-26660-7

[21] Hashemzadeh, S.M., Hosseini, S.H., Babaei, E., Sabahi, M.: Design and modelling of a new three winding coupled inductor based high step-up DC–DC converter for renewable energy applications. IET Power Electron.15, 1322–1339 (2022). https://doi.org/10.1049/pel2.12307

[22] Hasanpour, S. A novel soft-switched trans-inverse ultra-high-gain DC/DC converter with low switch voltage stress. Sci Rep 15, 31545 (2025). https://doi.org/10.1038/s41598-025-17301-w

[23] Tehranidoost Tabrizi, M.H., Sabahi, M., Bannae Sharifian, M. et al. Modified design TWCI-based high step-up DC-DC converter with reduced elements and low input current ripple for renewable applications. Sci Rep 16, 8037 (2026). https://doi.org/10.1038/s41598-026-37346-9

[24] Luo, P., He, J., Ji, H., Li, F., Jiang, H., Shi, L., Chen, G.: A high step-Up DC-DC converter based on three-winding coupled inductor and voltage multiplier for renewable energy applications. IET Power Electron.16, 961–974 (2023). https://doi.org/10.1049/pel2.12443

[25] Rostami, R., Hosseini, S.H. & Sharifian, M.B.B. High gain non-isolated step-up DC-DC converter proper for renewable energy applications. Sci Rep 15, 43608 (2025). https://doi.org/10.1038/s41598-025-26770-y